Insights of warm cloud biases in CAM5 and CAM6 from the single-column modeling framework and ACE-ENA observations

Yuan Wang[1,4,*], Xiaojian Zheng[2], Xiquan Dong[2], Baike Xi[2], and Yuk L. Yung[3]

[1]Department of Earth, Atmosphere, and Planetary Sciences, Purdue University, West Lafayette, IN, USA

[2]Department of Hydrology and Atmospheric Sciences, University of Arizona, Tucson, AZ, USA

[3]Division of Geological and Planetary Sciences, California Institute of Technology, Pasadena, CA, USA

[4]Now at Department of Earth System Science, Stanford University, Stanford, CA, USA

*Corresponding author: Yuan Wang (yzwang@stanford.edu)

Abstract

There has been a growing concern that most climate models predict too frequent precipitation, likely due to lack of reliable sub-grid variability and vertical variations of microphysical processes in low-level warm clouds. In this study, the warm cloud physics parameterizations in the singe-column configurations of NCAR Community Atmospheric Model version 6 and 5 (SCAM6 and SCAM5, respectively) are evaluated using ground-based and airborne observations from the DOE ARM Aerosol and Cloud Experiments in the Eastern North Atlantic (ACE-ENA) field campaign near the Azores islands during 2017-2018. Eight-month SCM simulations show that both SCAM6 and SCAM5 can generally reproduce marine boundary-layer cloud structure, major macrophysical properties, and their transition. The improvement of warm cloud properties from CAM5 to CAM6 physics can be found compared to the observations. Meanwhile, both physical schemes underestimate cloud liquid water content, cloud droplet size, and rain liquid water content, but overestimate surface rainfall. Modeled cloud condensation nuclei (CCN) concentrations are comparable with aircraft observed ones in the summer but overestimated by a factor of two in winter, largely due to the biases in the long-range transport of anthropogenic aerosols like sulfate. We also test the newly recalibrated autoconversion and accretion parameterizations that account for vertical variations of droplet size. Compared to the observations, more significant improvement is found in SCAM5 than in SCAM6. This result is likely explained by the introduction of sub-grid variations of cloud properties in CAM6 cloud microphysics, which further suppresses the scheme sensitivity to individual warm rain microphysical parameters. The predicted cloud susceptibilities to CCN perturbations in CAM6 are within a reasonable range, indicating significant progress since CAM5 which produces too strong aerosol indirect effect. The present study emphasizes the importance of understanding biases in cloud physics parameterizations by combining SCM with in situ observations.

1. Motivation and Background

Marine boundary-layer (MBL) clouds are crucial for the global radiation budget, as they efficiently regulate the solar radiation reaching the ocean surface (Dong et al., 2022) and largely determine the climate sensitivity (Sherwood et al., 2020). However, numerical simulations of MBL clouds in global climate models (GCM) remain challenging, mainly due to the mismatch of the spatial scales of MBL clouds (tens of meters) and GCM grids (~ 100 km). Therefore, empirical parameterizations of subscale cloud properties and variabilities, for both microphysics and macrophysics, play a critical role in predicting MBL clouds and precipitation in GCM (Wang et al., 2013). Consequently, how to constrain and improve those cloud parameterizations using the state-of-the-art observations become an important issue. One challenging aspect of the GCM cloud evaluation lies in the tight coupling between cloud physics and dynamics, as cloud microphysics can feedback to dynamics and thermodynamics through heating profile alteration or radiation flux interference (Wang et al., 2014, 2020).

To better probe the uncertainty source in the cloud physical parameterizations, a simplified GCM configuration has been developed to separate cloud physics from large-scale dynamical and thermodynamical conditions. The so-called single column model (SCM) is ideal for utilizing in situ observations from the field campaigns that are normally conducted intensively over the targeted area (Zhao et al., 2021). The modeling framework adopted in this study, NCAR Community Earth System Model (CESM), has a long history of providing such a modeling tool along with the development of its comprehensive models (Liu et al., 2007; Gettleman et al., 2019). With more added features and enhanced representations of cloud and aerosol in the cloud physical parametrizations in CESM version 1 and 2, it is valuable to evaluate the single-column versions of them using the recent field measurements.

The Eastern North Atlantic (ENA) is an ideal place around the world to study MBL clouds, considering the prevailing MBL cloud occurrence, diverse mesoscale meteorological conditions (Jensen et al., 2021; Zheng et al., 2022a), and distinctive aerosol sources (Wang, J. et al., 2021). A recent field campaign, the Aerosol and Cloud Experiments in the Eastern North Atlantic (ACE-ENA) provide ample ground-based and in situ aircraft observations of cloud micro- and macrophysics, aerosol properties, as well as atmospheric states over a whole summer and winter (Wang, J. et al. 2021; Wu et al., 2020). Recent WRF large-eddy simulations (LES) driven by the ERA5 reanalysis over the ENA well reproduce the general vertical variations of meteorological

factors and cloud cellular structure (Wang et al., 2020). Meanwhile, LES and observations exhibit substantial discrepancies in the evolution of MBL clouds in two selected stratocumulus cases during the ACE-ENA field campaign, likely due to the biases in both warm cloud physical parameterizations and meteorological conditions as external forcing. Those issues motivate us to look for stronger observational constraints in the single-column framework which minimizes the propagated errors from large-scale forcing. In this study, we use the ARM 3-hourly large-scale forcing of atmospheric states specifically developed for the ACE-ENA Intensive Observation Periods (IOP) to drive SCM.

The uncertainties of warm cloud physics in the atmospheric component of CESM1/2 have been reported in many previous studies (e.g. Kay et al., 2016; Zhao et al., 2022), while most of them focused on addressing the issues on the global scale. Leveraging the continuous radar retrievals of MBL cloud and drizzle microphysical properties during ACE ENA, Dong et al. (2021) modified the parameterizations of two key processes in warm cloud microphysics in CAM5, i.e., autoconversion from cloud droplets to rain drops and accretion of cloud droplets by raindrops. They showed that by applying this set of new parameterizations to CAM5 in global climate simulations, precipitation frequency is generally reduced but with enhanced intensity mainly in the mid-latitude regions, alleviating the long-lasting issue in the climate models, e.g., "too frequent and too light precipitation". Even the cloud radiative effect and top-of-atmosphere radiative flux simulations can be improved consequently. Meanwhile, a remaining question lies in whether such a new scheme works well over the location where the radar observational constraints come from originally. The single-column modeling framework enables us to examine the effect of the modified microphysical scheme on the local scale.

2. Methodology

2.1 Single column version of Community Atmospheric Model

In this study, we use single-column configuration of Community Atmospheric Model version 6 (referred to as SCAM6 thereafter) in the Community Earth System Model (CEMS 2.1.1). NCAR CESM is a community GCM that has been widely used to study the climate change (e.g. Yeager et al., 2018), precipitation extremes (e.g. Wang et al., 2016), cloud processes (e.g. Kay et al., 2012), and aerosol-cloud-radiation-circulation feedbacks in the Earth system (e.g. Wang et al., 2015). The atmosphere component of CESM2 (CAM6) has been modified substantially with a range of enhancements and improvements for the representation of physical processes since its last

version, CAM5. In particular, the modifications on the aerosol and cloud parameterizations are extensive. For example, a multivariate PDF-based third-order turbulence closure parameterization scheme, Cloud Layers Unified By Binormals (CLUBB), is implemented to unify the representation of boundary layer, shallow convection, and stratiform macrophysics in the model (Bogenschutz et al., 2013; Golaz and Larson, 2002). The two-moment cloud microphysical scheme is updated to version 2 (MG2, Gettelman and Morrison, 2015) with warm rain parameterization remaining as the Khairoutdinov & Kogan (2000) scheme (hereafter called KK). Major updates on cloud microphysics include prognostic precipitation (rain and snow), sub-stepping technique, and re-tuned autoconversion scheme which is critical for aerosol indirect effect on cloud lifetime and precipitation (Malavelle et al., 2017). The strong coupling between CLUBB and MG2 also enables interactions between subgrid shallow cloud, aerosol, and environment. Deep convection remains parameterized by the Zhang-McFarlane (1995) scheme and has been re-tuned to increase the sensitivity to convective inhibition. Parameterizations of homogeneous ice nucleation and heterogeneous immersion nucleation in cirrus clouds (Liu and Penner, 2005) explicitly consider the effects of sulfate and dust aerosol serving as ice nuclei on the cold clouds.

The Modal Aerosol Module (MAM) in CESM is updated from a three-mode to four-mode approach (MAM4) to better consider the aging processes of black carbon in the atmosphere (Liu et al., 2016; Wang et al., 2018). Six types of aerosols with different hygroscopicity and optical properties are considered in MAM3, including sulfate, black carbon (BC), primary organic matter (POM), secondary organic aerosol (SOA), dust and sea salt. The aerosol module accounts for most of the important processes associated with atmospheric aerosols, including emission, nucleation, coagulation, condensational growth, gas and aqueous-phase chemistry, dry deposition, in-cloud and below-cloud scavenging, re-production from evaporated cloud droplets and suppression, as well as agricultural, deforestation, and peat fires (Li and Lawrence, 2017). To test the impacts of cloud physical parameterization on the model fidelity, we also conduct the single-column simulations using the CAM5 physics (SCAM5) under the same large-scale forcing data.

Because the ACE-ENA is a relatively new field campaign and does not have a pre-defined case in SCAM6, we create a new case in CAM6 based on a new set of large-scale data for this IOP. The large-scale forcing over the ARM-ENA is developed from the constrained variational analysis (VARANAL, Xie et al., 2004; Tang et al., 2019). It includes air temperature (T) and moisture (q), their horizontal and vertical advection, surface sensible and latent heat fluxes, U and

V winds, large-scale vertical motion/velocity, TOA/surface radiation fluxes, etc. VARANAL is based on ERA5 reanalysis (Copernicus Climate Change Service, 2017) with the additional input of observations from the ARM ENA site incorporated into the variational analysis, to represent the atmospheric states over a Global Climate Model (GCM) grid box. The original VARANAL data is produced specifically for the ACE-ENA IOP, with a temporal resolution of 3-hour and 45 vertical levels.

To minimize the biases in aerosol advection and dynamical forcing, aerosol and the temperature fields are nudged to their initial conditions on different timescales, varying from 10 days at the bottom of the model to 2 days at the top of the model (Gettelman et al., 2019). Also, to simulate the right seasonal variations of aerosol and temperature initial conditions, each of our model integration only lasts one month, and a new sequential run will follow with updated initial conditions. By doing so the seasonality of aerosols will follow that of climatology on the monthly basis. CAM6 model has 32 vertical levels from the surface to 2 hPa (about 45 km), while CAM5 have 30 levels. The two models both use a time step of about 30 minutes, while CAM6 uses sub-stepping for microphysical processes.

2.2 Numerical experiment design

To cover the full IOP in our simulations, we run SCAM5 and SCAM6 over 8 months from June 1, 2017, to Feb 1, 2018, as control experiments (Ctrl). To explore the possible sources of biases in simulated drizzle and LWC, we employ a retuned KK scheme (Dong et al., 2021, thereafter as D21-KK) that explicitly links the autoconversion and accretion rates with mass mean cloud droplet radius ($r_{m,c}$). The original KK scheme is expressed as below:

$$R_{auto}(Z) = \left(\frac{\partial q_r}{\partial t}\right)_{auto} = A\, q_c^{a1}(Z) N_c^{a2}, \quad (1)$$

and,

$$R_{accr}(Z) = \left(\frac{\partial q_r}{\partial t}\right)_{accr} = B\, \left(q_c(Z) q_r(Z)\right)^b, \quad (2)$$

where A = 1350, $a1$ = 2.47, and $a2$= -1.79 in CAM5. In D21-KK, both autoconversion and accretion rates are further aware of the vertical variations of r_c, so the constant A and B are replaced as a function of r_c:

$$R'_{auto}(Z) = \frac{RLWC(Z)}{\int \rho_{air} P_r(Z) dt} R_{auto}(Z) = A'(Z) q_c^{2.47}(Z) N_c^{-1.79}, \quad (3)$$

and,

$$R'_{accr}(Z) = \frac{RLWC(Z)}{\int \rho_{air} P_r(Z) dt} R_{accr}(Z) = B'(Z)\left(q_c(Z) q_r(Z)\right)^{1.15}, \quad (4)$$

where A' and B' are further parameterized in CAM5 as:

$$A'(Z) = 121683 \times exp\left(-0.528\, r_{m,c}(Z)\right) + 364, \quad (5)$$

and,

$$B'(Z) = 632 \times exp\left(-24.5 \frac{r_{m,c}(Z)}{r_{m,r}(Z)}\right) + 51, \quad (6)$$

CAM6 microphysics aims to reduce the autoconversion dependency on the N_c, so $a2$ and A are set as -1.1 and 13.5, respectively, with $a2$ unchanged. We did the same recalibration for CAM6 autoconversion processes, and the corresponding A' is parameterized as:

$$A'(Z) = 3359 \times exp\left(-0.721\, r_{m,c}(Z)\right) + 8, \quad (7)$$

Hence the updated autoconversion for CAM6 microphysics has the form as below:

$$R'_{auto}(Z) = \frac{RLWC(Z)}{\int \rho_{air} P_r(Z) dt} R_{auto}(Z) = f_e\, A'(Z) q_c^{2.47}(Z) N_c^{-1.1}, \quad (8)$$

Where f_e represents an enhancement factor which is diagnosed from the CLUBB to account for sub-grid variabilities of cloud and rain.

In another set of sensitivity experiment, to explore the aerosol indirect effect on cloud and warm precipitation, we scale up aerosol number and mass concentrations in the accumulation mode by a factor of 2 in the initial condition. Such an experiment is named as "pAero". Moreover, to examine the sensitivity of cloud simulations to the large forcing data, we perturb specific humidity state variable and related tendency terms, with an experiment name "ForcingQ_Adj". All the above experiment are summarized in Table 2.

2.3 ACE-ENA observations

Aircraft in situ observations during the ACE-ENA provide best available characterizations of cloud and aerosol vertical distributions, with differentiation of aerosol types and hygroscopicity. During the two IOPs, 39 flights were deployed to collect data for 39 days, 20 in the summer IOP, 19 in the winter IOP. Meanwhile, ground-based observations were conducted simultaneously and consecutively. Based on the Ka-band ARM Zenith Radar (KAZR) measurements, cloud and rain microphysical properties (cloud droplet effective radius, r_c; cloud droplet number concentration, N_c; cloud liquid water content, $CLWC$; rain droplet mass median radius, $r_{m,r}$; rain droplet number concentration, N_r; and rain liquid water content, $RLWC$) over the ARM ENA site can be retrieved

(Wu et al. 2020). The cloud and drizzle microphysical retrievals were validated by the aircraft in situ measurements from ACE-ENA field campaign, with the estimated median uncertainties of ~15% for r_c, ~30% for $r_{m,r}$, ~30% for N_c and $CLWC$, and ~50% for N_r and $RLWC$. Note that the subscript "c" denotes cloud and subscript "r" denotes rain. The model counterparts are extracted and compared with the retrieval, except the $r_{m,r}$ which is not an output from the model. Following the method in Wu et al. (2020) equation 2a, the $r_{m,r}$ can be calculated by:

$$r_{m,r} = \left(\frac{RLWC*3.67^4}{\rho_w*N_W*8\pi}\right)^{1/4} \quad (9).$$

where the ρ_w is water density, and the N_W is the normalized drizzle number concentration ($N_W = N_r/r_{m,r}$). Furthermore, the $CLWC$ ($RLWC$) is scaled by the cloud (rain) fraction within the grid box to match the retrievals.

For the aircraft in situ measurements of aerosol, the Passive Cavity Aerosol Spectrometer (PCASP) measured the aerosols with the size range from 0.1 μm to 3.2 μm (Goldberger, 2020), hence the accumulation-mode aerosol number concentration (N_{Acc}) can be derived from the PCASP 0.1 μm to 1.0 μm measurement. The CCN number concentration (N_{CCN}) is obtained by the CCN-200 particle counter on board the G-1 aircraft. The N_{CCN} is a measurement under the controlled supersaturation of 0.35 % with a humidified particle size range from 0.75 to 10 μm (Uin and Mei, 2019). The PM1 aerosol chemical components mass concentrations are measured by the Aerodyne High-Resolution Time-of-Flight Aerosol Mass Spectrometer (HR-ToF-AMS). The accuracy of each individual instrument can be found in the instrument handbooks available on the ARM website.

We select only those research flights that followed a horizontal track within one grid size of the CAM models (1.25° longitude and 0.9° latitude), centered on the ARM ENA site. Also, to meet the criteria for comparison with SCAM, each aircraft case must include comprehensive vertical sampling of cloud and aerosol within the specified time period. To ensure the apple-to-apple comparison between model and observations, the cloud and rain samples are selected following the same criteria: 1) $4\ \mu m < r_c < 25\ \mu m$; 2) $CLWC > 0.01\ gm^{-3}$; 3) $N_c > 1\ cm^{-3}$; and 4) $RLWC > 1 \times 10^{-4}\ gm^{-3}$. The geopotential height from the model output is extracted for each time step, hence the quantities at pressure level can be converted to height level and compared with the observation results. Both model and observation results are limited to below 3km.

3. Evaluation of SCAM using ACE-ENA observations

3.1 Meteorological conditions

To understand the cloud and drizzle property differences between simulations and observations, we first evaluate the SCAM6 simulated meteorological conditions by the ARM Interpolated Sonde (INTERPSONDE) value-added product (VAP), which is an independent dataset from the large-scale forcing data used to drive SCM. As shown in Fig. 1a, the simulated air temperature (T_{air}) values are generally comparable to the observed ones with clear seasonal variations. The statistics from the 8-month simulations shows that the differences in both mean and median T_{air} agree within 1% to the observed ones (Fig. 1c). However, the probability distribution functions (PDF) reveal some cancelling effect behind the good agreement on the means: the simulated values over the temperature "extremes" (lower and higher bins) are larger than the observed ones, but in the middle bins, the observed values surpass the simulated ones (for the bins between 280 and 290 K). Essentially, the modeled T_{air} PDF is wider than the observed one. The discrepancy of the moisture field is more evident. Even though the model captures the evolution of relative humidity (RH) throughout 8 months, both mean and median RH have ~10% bias in the model. In particular, the biases become severe when RH values fall into the high humidity regime. The RH frequency within the 90-100% range is about two times higher in SCAM6 than the observations. A comparison of specific humidity (SH) shows that SCAM6 overpredicts SH by 11.8%, indicating that the RH bias stems mainly from the absolute moisture bias. The similar statistics for the grids with RH larger than 90% shows the discrepancy in SH is still larger than that of T_{air} (Fig. S1), indicating larger contribution of SH to RH biases than T_{air}. It can be explained by the fact that temperature field is relaxed to the input as an additional constraint, while SH is predicted as a fully prognostic variable in SCM. We will examine the potential impact of moisture uncertainty in the large-scale forcing data on the cloud property simulation through sensitivity, and the results will be discussed below.

3.2 Cloud properties

We first compare CLWC and RLWC over time and altitude dimensions between SCAM6 simulations and ARM radar-lidar-MWR retrievals (Figure 2a-d). The simulated CLWC values in both time and altitude are generally consistent with the ARM retrievals. More specifically, SCAM6 can capture those vertically thick clouds in early November and middle December due to the prevalent frontal systems during that time of the year. However, some high CLWC values are not reproduced in the model. Similarly, the temporal evolution of simulated RLWC agrees with the

retrievals as demonstrated in Figure 2c-d, however, their magnitudes are much lower than the retrievals. The relatively coarse vertical resolution near the planetary boundary layer (PBL) is discernable from the discretized cloud vertical distribution in the model simulations (Fig. 2a, c). However, the vertical development of different cloud types (stratus, stratocumulus, and cumulus) and their transitions are generally reproduced by SCAM6. When cumulus occurs with cloud top height greater that 2000 m, the model can always capture them. Despite good agreement on cloud top height, SCAM6 overpredicts CLWC and RLWC frequency near the surface (< 200 m) compared to the observations. The statistics of cloud macrophysics in Fig. 3 supports the analyses above. Cloud top heights show good agreement between SCAM6 and observations, with 8-month mean values of 1561 m and 1425 m, respectively (Fig. 3f). It corroborates the notion that SCAM6 can capture the cloud type transition relatively well. However, due to the lower cloud-base height in SCAM6, cloud physical thickness is overestimated in the model. Even with the above biases in cloud macrophysics, the modeled cloud mass center (CMC) height (mean cloud layer heights weighted by CLWC) is comparable to the observed ones (Fig. 3h).

A further comparison of 8-month surface precipitation rate in Fig. 2e and 2f shows that SCAM6 can capture the heavy precipitation (>25 mm/day) under the large-scale forcing during the winter season (Oct. to Jan.). However, the "too-frequent-drizzle" issue persists throughout the 8-month simulations. The frequency of light precipitation (< 2 mm/day) is more than 80% which is rather unrealistic compared to the observations. The mean surface precipitation in SCAM6 is overestimated by 30% compared to the rain gauge measurements during the whole 8-month period.

The statistical comparisons of cloud and drizzle microphysical properties in Fig. 3a-d reveal that CLWC is overestimated by about 30%. Consequently, r_c is slightly larger in the model, and the bias becomes worse for those larger droplets (r_c greater than 10 micron). Too large CLWC fosters fast cloud to warm rain conversion, but the simulated RLWC values are smaller than the retrievals, leading to too frequent surface precipitation mainly in the drizzle form. Note that retrieved RLWC from ground-based radar also bears with large uncertainty, as indicated by the large error bar in Fig. 3c. Hence the real differences of RLWC between SCAM6 and observations remain hard to be quantified. Our analyses here include all 8-month simulation results and all types of cloud. In an additional analysis, by focusing on the marine boundary layer (MBL) stratiform cloud only, we obtain quite similar cloud evaluation results. As shown in Fig. S2, then we strengthen our selection criteria by only sampling consecutive cloud layers lasting more than 2

hours with the cloud top height less than 3 km, the statistics of cloud micro- and macro- physical properties do not differ significantly. It reflects the fact that over the ENA, MBL clouds are predominated during those seasons. In observation of the SH bias against observations (Fig. 1), additional SCAM6 sensitivity test is conducted by perturbing moisture content and the associated advection with a scaling factor of 0.85. Results show that the distributions of simulated SH and RH only slightly shift towards the lower tail with smaller mean values, which cannot correct their biases. Notably, despite the minor changes in the simulated cloud and drizzle microphysics, the cloud top height, thickness, and CMC simulations perform noticeably better than the control simulation (Fig. S3). It suggests that the moisture fields in the large-scale forcing exert larger impacts on the simulated cloud structure and macrophysics than the microphysics. In other words, cloud microphysical properties are strongly regulated by the parameterizations in the model, and less sensitive to the external forcing.

Driven by the same large-scale forcing, SCAM5 simulated meteorological fields are similar to SCAM6 (Fig. S4), but cloud properties are quite different from those by SCAM6. Instead of an overestimation in SCAM6, the SCAM5 simulated CLWC exhibits an underestimation (Fig. 4a). One possible reason is the change of formula for the saturation vapor pressure in the MG2 cloud microphysics scheme (Gettelman and Morrison, 2015). Previous SCM simulations for the MPACE case also show the larger LWC by MG2 than MG1 (Gettelman et al., 2015). The good agreement of the mean r_c in SCAM6 does not exist in the SCAM5 simulations (Fig. 4b), and too many small cloud droplets (less than 6 micron) are present in SCAM5, which are not found in either observation or SCAM6. RLWC in SCAM5 is still much smaller than observations (Fig. 4c), suffering the similar issue to SCAM6. Different from SCAM6, SCAM5 overpredicts mean $r_{m,r}$ (Fig. 4d) but underpredicts mean r_c. The high bias in drizzle size is likely related to the too strong raindrop accretion process, while the low bias in drizzle amount is subject to both source and sink uncertainty with the drizzle budget. The mean surface precipitation in SCAM5 is 0.082 mm/day (Fig. S5), higher than the 0.056 mm/day in observation and 0.073 in SCAM6. The anomalously high surface precipitation lines up with too large drizzle size and too low drizzle amount suspended in the air in SCAM5.

The improvement of the cloud macrophysics from SCAM5 to SCAM6 is more evident than that of microphysics. Too low cloud-base height and cloud-top height result in too thin cloud deck in SCAM5 (Fig. 4e-g). The cloud center mass is also systematically low in SCAM5. By and large,

the updated cloud physics in CAM6 helps improve many aspects of cloud simulations, but the drizzle issues still linger on.

3.3 Aerosols

To probe the possible uncertainty sources for cloud droplet number concentration, vertical profiles of aerosol and CCN number concentrations are compared between SCAM6 simulations and in situ aircraft observations from 17 flights near the Azores islands during the ACE-ENA field campaign (Fig. 5). The in situ profiles represent the average of data collected during 12 flights and 5 flights selected during the summer and winter IOPs, respectively. The SCAM6 profiles correspond to the averages within the 17-flight time-stamps. SCAM6 generally gets seasonality right, i.e., aerosol and CCN number concentrations are high in summer and low in winter. The model also agrees with observations on the magnitude of accumulation-mode aerosol concentration (N_{ACC}) and CCN concentration (N_{CCN}) during the summer, which further leads to a reasonable comparison of N_C. The small bias of N_C generally follows the performance of N_{CCN}, i.e., high bias near the bottom while low bias near the top. One intruiguing phenomenon during the summertime is that N_{CCN} can be even higher than N_{ACC}, found in both aircraft measurements and model simulations. The high N_{CCN} occurs within the MBL (<1000 m) in SCAM6. In contrast, measured N_{CCN} in lower free troposphere (FT, 2000-2500 m) is of the same magnitude with that within MBL, and FT N_{CCN} is higher than N_{ACC}in the observations. A breakdown of aerosol number concentration budget in SCAM6 (Fig. S6) shows that Aitken-mode aerosols contribute to about 20% summertime and 45% wintertime total aerosol numbers. In contrast, the coarse-mode aerosol number is only about 1% of the Aitken-mode one. Therefore, the large N_{CCN} within the MBL in SCAM6 should be attributed to the efficient Aitken-mode aerosol activation near the cloud bottom in SCAM6. A further examination of aerosol chemical compositions in SCAM6 suggests that sulfate is the predominated aerosol species in the Aitken mode (Fig. S7).

Understanding larger N_{CCN} than N_{ACC} in the lower FT in the observations is challenging, because coarse- and Aitken- mode aerosol number concentrations was not measured during the IOP. However, previous study found that new particle formation frequently occurs in the FT over the ENA, because of the sulfuric acids being elevated, especially during summertime where the oceanic dimethyl sulfide (DMS) emissions are strong (Zawadowicz et al., 2021). Previous back-trajectory analyses by Wang et al. (2020) suggest the long-range transport of the fine-mode aerosols to the ENA site likely originates from the continental U.S. Therefore, the oxidations of

DMS, jointly with the long-range transported pollution, contribute to the elevated Aitken-mode aerosol concentrations in the FT. Those Aitken-mode aerosols (e.g., DMS oxides and diluted continental pollutants) are found to be substantial contributors to the CCN budget (Wang et al., 2021). The FT aerosols and CCN can be further entrained down to the MBL, consistent with what is shown in Fig. 5. Note that SCAM6 predicts the "top-heavy" Aitken model aerosol concentration profile, but it does not lead to the larger N_{CCN} above the MBL. Hence, we can only speculate that in the real atmosphere, there are significant Aitken mode aerosols that can serve as CCN in the lower FT, but that is not the case in SCAM6. The above discussions reinforce the notion that it is crucial to accurately simulate the long-range transport of aerosols and their growth over a remote maritime region like ENA. And future investigation on how the aerosol activation process is simulated in different model levels is warranted.

During the winter, N_{ACC} is comparable between model and observation (Fig. 5d), while $N_{CCN}$is significantly overestimated from the surface to 2000 m altitude (Fig. 5e). Based on our analyses above for the summer, we can infer that too strong contribution from the Aitken mode to the CCN budget also exists in winter. Moreover, there is a non-negligible effect that the frequent convective activities and associate large super saturation within the mid-latitude frontal systems during wintertime also likely result in the stronger activation of Aitken mode aerosol. Surprisingly, the modeled N_C shows good agreement with observations, despite the overestimated N_{CCN}. One plausible reason is the canceling effect from the too strong N_C sink in the model. The overestimated cloud droplet size by the model (Fig. 3b) fosters the warm rain formation, and in turn, efficiently deplete cloud droplets (Zheng et al., 2022b), keeping the modeled N_C at a comparable level with the observations.

4. Impacts of new observation-constrained warm rain parameterizations

Our previous study showed that this set of new parameterizations in CAM5 help alleviate the long-lasting issue in the climate models, e.g., "too frequent and too light precipitation", on the global scale (Dong et al., 2021). When we apply the same set of parameterizations in SCAM5 over the ENA (referred to as $\text{SCAM5}_{\text{D21}}$), we find similar improvements on cloud and precipitation properties. As shown in Fig. 6, CLWC in $\text{SCAM5}_{\text{D21}}$ is elevated due to the less efficient autoconversion scheme, and the simulated CLWC values agree better with the ARM retrievals compared with original SCAM5. r_c is also enlarged in $\text{SCAM5}_{\text{D21}}$, being more consistent with retrievals. The mass median radius of raindrops $r_{m,r}$ are reduced slightly, while there is no

significant change in RLWC in $SCAM5_{D21}$. Because of the improved cloud microphysical properties, cloud macrophysics also match up better with observations. Cloud base height, cloud top height, and cloud mass center height are all improved to some extent in $SCAM5_{D21}$ simulations (Fig. 6e-h). These comparisons are encouraging, indicating that the D21-KK new warm parameterizations in SCAM5 make significant improvements on the simulated MBL cloud and drizzle properties.

Different from the CAM5 microphysics, CAM6 starts to introduce sub-grid cloud variations (Lebsock et al., 2013; Zhang et al., 2020) and re-tuned the parameters in the KK2000 scheme. One direct consequence is that CLWC has been changed from underestimation to overestimation (Fig. 7a). Therefore, an even slower autoconversion process with the new D21-KK scheme cannot further benefit the warm rain processes in CAM6. As expected, $SCAM6_{D21}$ does not exhibit improvement in simulating both cloud microphysics and macrophysics (Fig. 7). Distinctive sensitivities to the same microphysical parameter modification under different versions of the physics package poses a challenge on model improvement through only updating a certain set of parameterizations.

5. Assessing aerosol indirect effects under the single-column frameworks

Aerosol indirect effects, especially the second indirect effect concerning the liquid water content change, was reported to be over-predicted in CAM5 when simulating the aerosol perturbations, such as volcano eruptions, on the low clouds (Malavelle et al., 2017). Here we assess the aerosol first and second indirect effects of CAM6 over the ENA under the single-column framework. To perturb the CCN budget, we choose to modify the accumulation-mode aerosols in their initial conditions. As the aerosol relaxation is on, such a perturbation is expected to constantly impact the aerosol field during the integrations. Considering the relatively low background aerosol concentration over ENA, the change in aerosol direct effect on the clear-sky radiation fluxes can be ignored in this setup. Both aerosol number and mass concentrations in the accumulation mode are enlarged by a factor of 2, the results are labeled as $S6_{pAero}$ and are compared with the original SCAM6 simulations (Fig. 8). With such an aerosol perturbation, N_{CCN} within MBL (< 1km) is increased from 112.5 to 175.8 cm^{-3}, corresponding to a 56% enhancement. Similarly, CCN in the lower FT and upper MBL (1-3 km) increased by 61%. Aerosol first and second indirect effects are evident in SCAM6, as reduced r_c and increased CLWC are both found in the perturbed experiment. We further quantify the droplet size susceptibility and cloud water susceptibility with respect to

MBL CCN changes by $\frac{\partial ln(r_c)}{\partial ln(N_{CCN})}$ and $\frac{\partial ln(CLWC)}{\partial ln(N_{CCN})}$, respectively. The SCAM6 simulated droplet size susceptibility is –0.2, close to the LES simulated range from –0.22 to –0.25 and the upper bound of the observed range over ENA (Wang et al., 2020; Zheng et al., 2022a). The SCAM6 simulated cloud water susceptibility is +0.19 which also falls into the LES prediction (+0.18 to +0.30). Those results suggest that the newly introduced sub-grid cloud variabilities in SCAM6 can account for the aerosol indirect effects at a reasonable level. Mean surface precipitation amount shows relatively small responses to CCN perturbation (less than 2%), because convective precipitation in early winter dominates the study period while deep convective parameterization in SCAM6 is still unlinked with cloud microphysics and unaware of CCN effects so far. Cloud top height (Z_T) shows an increase with higher CCN concentration (Fig. 8f), likely due to the enhanced latent heat release following the elevated condensational rate.

6. Conclusion and Discussion

The single-column versions of NCAR CAM5 and CAM6 are employed to simulate marine boundary-layer cloud and aerosol properties over the eastern North Atlantic during the ACE-ENA field campaign and to assess the uncertainty in cloud microphysical parameterizations. 3-hourly large-scale forcing data are derived from the systematic measurements of atmospheric states during the 8-month IOP. SCAM6 well reproduces the temperature field but overestimates specific and relative humidity by about 10%, especially for those near-cloud grid points. Our moisture adjustment simulation suggests that moisture variables in the large-scale forcing exert larger impacts on simulated cloud structures than cloud microphysics. It further implies that cloud microphysical properties are strongly regulated by the parameterizations, and less sensitive to the external forcing. Cloud frequency and transition between different types show good agreement between SCM and observation. Cloud simulations are generally improved from SCAM5 to SCAM6, in terms of droplet effective radius, cloud top height, and cloud thickness. However, there are some common issues with warm precipitation in those two models, concerning too small rainwater content and too frequent surface light precipitation.

To probe the possible contributions from the warm cloud parameterization to those drizzle biases, we implement the recalibrated autoconversion and accretion processes in the KK scheme for both SCAM5 and SCAM6. The updated parameterziations explicitly consider vertical variations of droplet size. The new scheme tends to improve CLWC and r_c in SCAM5 as well as $r_{m,r}$, but does not significantly alleviate the drizzle problem. The improvement is absent in

SCAM6, likely because sub-grid variations of cloud properties have been introduced in CAM6 cloud microphysics (especially for the autoconversion parameterization), suppressing the KK scheme sensitivity to other factors. Further study is warranted to test whether the same warm rain precipitation sensitivity holds for different cases using SCAM5/6.

Aerosol simulations in SCAM6 are evaluated against the aircraft measurements during the ACE-ENA. Significant Aitken-mode aerosol contribution to the CCN budget over ENA is identified in both models and observations. SCAM6 agrees with observations on the magnitude of concentration of accumulation-mode aerosol, CCN, and cloud droplets during the summer, while N_{CCN} is significantly biased high from the surface to 2000 m in altitude during the winter. Aerosol budget analyses show that in SCAM6, long-range transport provides too many Aitken-mode sulfates that entrain into the MBL and can grow to CCN-size particles consequently. We further quantify aerosol indirect effects by perturbing accumulation-mode aerosol concentrations in the model. SCAM6 predicted cloud water and droplet size susceptibilities line up with the classic CCN effects, i.e., reduced droplet size but enhanced liquid water content under the high CCN scenario. The magnitudes of the cloud water and droplet size susceptibilities are also close to the LES simulations conducted for the selected cases during the ACE-ENA.

The present study provides new insight of model biases in aerosol and warm cloud simulations in the NCAR CAM models. Different from the previous evaluations of a full model run with potential large biases propagated from modeled large-scale conditions, the model biases discussed here, especially the drizzle property issue, should be adequately addressed in the future development of CAM. The existing progress of predicted cloud properties and aerosol effects is clearly demonstrated under the single-column framework in this study. More comprehensive aerosol measurements, including Aitken- and coarse- mode aerosol properties, are needed in the future field campaign to better understand the aerosol budget and aerosol-cloud interactions.

Code availability

The code of CESM model used in this study is available at https://www.cesm.ucar.edu/models/cesm2/release_download.html.

Data availability

All the CESM model simulation input and output used for this research can be downloaded from

the website at http://web.gps.caltech.edu/~yzw/share/Wang-2023-SCM. The aircraft and ground-based measurements used in this study were obtained from the Atmospheric Radiation Measurement (ARM) Program sponsored by the U.S. Department of Energy (DOE) Office of Energy Research, Office of Health and Environmental Research, and Environmental Sciences Division. The measurement data can be downloaded from http://www.archive.arm.gov/.

Competing interests

Yuan Wang is a member of the editorial board of Atmospheric Chemistry and Physics.

Acknowledgement

This study was primarily supported by the collaborative NSF grant (Award No. AGS-2031751, 2031750). We thank the instrument mentors of the instruments and the individuals collecting measurements during the ACE-ENA field campaign. We also acknowledge high-performance computing support from NCAR Cheyenne. All requests for materials in this paper should be addressed to Yuan Wang (yzwang@stanford.edu).

References

Bogenschutz, P. A., Gettelman, A., Morrison, H., Larson, V. E., Craig, C., and Schanen, D. P.: Higher-Order Turbulence Closure and Its Impact on Climate Simulations in the Community Atmosphere Model, J. Climate, 26, 9655-9676, 10.1175/JCLI-D-13-00075.1, 2013.

Copernicus Climate Change Service (C3S): ERA5: Fifth generation of ECMWF atmospheric reanalyses of the global climate. Copernicus Climate Change Service Climate Data Store (CDS), available at https://cds.climate.copernicus.eu/cdsapp (last access:), 2017.

Dong, X., Wu, P., Wang, Y., Xi, B., and Huang, Y.: New Observational Constraints on Warm Rain Processes and Their Climate Implications, Geophys. Res. Lett., 48, e2020GL091836, https://doi.org/10.1029/2020GL091836, 2021.

Dong, X., Zheng, X., Xi, B., and Xie, S.: A climatology of mid-latitude maritime cloud fraction and radiative effect derived from the ARM ENA ground-based observations, J. Climate, 1-31, 10.1175/JCLI-D-22-0290.1, 2022.

Gettelman, A. and Morrison, H.: Advanced Two-Moment Bulk Microphysics for Global Models. Part I: Off-Line Tests and Comparison with Other Schemes, J. Climate, 28, 1268-1287, https://doi.org/10.1175/JCLI-D-14-00102.1, 2015a.

Gettelman, A., H. Morrison, S. Santos, P. Bogenschutz, and P. M. Caldwell: Advanced Two-Moment Bulk Microphysics for Global Models. Part II: Global Model Solutions and Aerosol–Cloud Interactions. J. Climate, 28, 1288–1307, https://doi.org/10.1175/JCLI-D-14-00103.1, 2015b.

Gettelman, A., Truesdale, J. E., Bacmeister, J. T., Caldwell, P. M., Neale, R. B., Bogenschutz, P. A., and Simpson, I. R.: The Single Column Atmosphere Model Version 6 (SCAM6): Not a Scam but a Tool for Model Evaluation and Development, Journal of Advances in Modeling Earth Systems, 11, 1381-1401, https://doi.org/10.1029/2018MS001578, 2019.

Golaz, J. C., Larson, V. E., and Cotton, W. R.: A PDF-based model for boundary layer clouds. Part I: Method and model description, J. Atmos. Sci., 59, 3540-3551, 2002.

Goldberger, L.: Passive cavity aerosol spectrometer probe aboard aircraft (PCASP-AIR) with signal processing package 200 instrument handbook, DOE/SC-ARM-TR-241, Available from: https://www.arm.gov/publications/tech_reports/handbooks/doe-sc-arm-tr-241.pdf, 2020.

Jensen, M. P., Ghate, V. P., Wang, D., Apoznanski, D. K., Bartholomew, M. J., Giangrande, S. E., Johnson, K. L., and Thieman, M. M.: Contrasting characteristics of open- and closed-cellular

stratocumulus cloud in the eastern North Atlantic, Atmos. Chem. Phys., 21, 14557-14571, 10.5194/acp-21-14557-2021, 2021.

Kay, J. E., and Coauthors: Exposing Global Cloud Biases in the Community Atmosphere Model (CAM) Using Satellite Observations and Their Corresponding Instrument Simulators. J. Climate, 25, 5190–5207, https://doi.org/10.1175/JCLI-D-11-00469.1., 2012.

Kay, J. E., Bourdages, L., Miller, N. B., Morrison, A., Yettella, V., Chepfer, H., and Eaton, B.: Evaluating and improving cloud phase in the Community Atmosphere Model version 5 using spaceborne lidar observations, J. Geophys. Res.-Atmos., 121, 4162-4176, https://doi.org/10.1002/2015JD024699, 2016.

Khairoutdinov, M. & Kogan, Y. A New Cloud Physics Parameterization in a Large-Eddy Simulation Model of Marine Stratocumulus. Mon. Weather Rev. 128, 229–243, 2000.

Lebsock, M., Morrison, H., and Gettelman, A., Microphysical implications of cloud-precipitation covariance derived from satellite remote sensing, J. Geophys. Res. Atmos., 118, 6521– 6533, doi:10.1002/jgrd.50347, 2013.

Li, F. and Lawrence, D. M.: Role of Fire in the Global Land Water Budget during the Twentieth Century due to Changing Ecosystems, J. Climate, 30, 1893-1908, https://doi.org/10.1175/JCLI-D-16-0460.1, 2017.

Liu, X. and Penner, J.E.: Ice Nuclei Parameterization for Global Model. Meteorologische Zeitschrift, 14, 499-514. https://doi.org/10.1127/0941-2948/2005/0059, 2005.

Liu, X., Penner, J. E., Ghan, S. J., and Wang, M.: Inclusion of Ice Microphysics in the NCAR Community Atmospheric Model Version 3 (CAM3), J. Climate, 20, 4526-4547, https://doi.org/10.1175/JCLI4264.1, 2007.

Liu, X., Ma, P. L., Wang, H., Tilmes, S., Singh, B., Easter, R. C., Ghan, S. J., and Rasch, P. J.: Description and evaluation of a new four-mode version of the Modal Aerosol Module (MAM4) within version 5.3 of the Community Atmosphere Model, Geosci. Model Dev., 9, 505-522, 10.5194/gmd-9-505-2016, 2016.

Malavelle, F. F., Haywood, J. M., Jones, A., Gettelman, A., Clarisse, L., Bauduin, S., Allan, R. P., Karset, I. H. H., Kristjánsson, J. E., Oreopoulos, L., Cho, N., Lee, D., Bellouin, N., Boucher, O., Grosvenor, D. P., Carslaw, K. S., Dhomse, S., Mann, G. W., Schmidt, A., Coe, H., Hartley, M. E., Dalvi, M., Hill, A. A., Johnson, B. T., Johnson, C. E., Knight, J. R., O'Connor, F. M., Partridge, D. G., Stier, P., Myhre, G., Platnick, S., Stephens, G. L., Takahashi, H., and

Thordarson, T.: Strong constraints on aerosol–cloud interactions from volcanic eruptions, Nature, 546, 485-491, 10.1038/nature22974, 2017.

Sherwood, S. C., Webb, M. J., Annan, J. D., Armour, K. C., Forster, P. M., Hargreaves, J. C., Hegerl, G., Klein, S. A., Marvel, K. D., Rohling, E. J., Watanabe, M., Andrews, T., Braconnot, P., Bretherton, C. S., Foster, G. L., Hausfather, Z., von der Heydt, A. S., Knutti, R., Mauritsen, T., Norris, J. R., Proistosescu, C., Rugenstein, M., Schmidt, G. A., Tokarska, K. B., and Zelinka, M. D.: An Assessment of Earth's Climate Sensitivity Using Multiple Lines of Evidence, Reviews of Geophysics, 58, e2019RG000678, https://doi.org/10.1029/2019RG000678, 2020.

Tang, S., C. Tao, S. Xie and M. Zhang: Description of the ARM Large-Scale Forcing Data from the Constrained Variational Analysis (VARANAL) Version 2, DOE ARM Climate Research Facility, Technical Report DOE/SC-ARM-TR-222. Available at: https://www.arm.gov/publications/tech_reports/doe-sc-arm-tr-222.pdf, 2019

Uin, J., and F. Mei: Cloud condensation nuclei particle counter instrument handbook – airborne version, DOE/SC-ARM-TR-225, Available from: https://www.arm.gov/publications/tech_reports/handbooks/doe-sc-arm-tr-225.pdf, 2019

Wang, J., Wood, R., Jensen, M. P., Chiu, J. C., Liu, Y., Lamer, K., Desai, N., Giangrande, S. E., Knopf, D. A., Kollias, P., Laskin, A., Liu, X., Lu, C., Mechem, D., Mei, F., Starzec, M., Tomlinson, J., Wang, Y., Yum, S. S., Zheng, G., Aiken, A. C., Azevedo, E. B., Blanchard, Y., China, S., Dong, X., Gallo, F., Gao, S., Ghate, V. P., Glienke, S., Goldberger, L., Hardin, J. C., Kuang, C., Luke, E. P., Matthews, A. A., Miller, M. A., Moffet, R., Pekour, M., Schmid, B., Sedlacek, A. J., Shaw, R. A., Shilling, J. E., Sullivan, A., Suski, K., Veghte, D. P., Weber, R., Wyant, M., Yeom, J., Zawadowicz, M., and Zhang, Z.: Aerosol and Cloud Experiments in the Eastern North Atlantic (ACE-ENA), B. Am. Meteorol. Soc., 1-51, 10.1175/BAMS-D-19-0220.1, 2021.

Wang, Y., Fan, J., Zhang, R., Leung, L. R. and Franklin, C.: Improving bulk microphysics parameterizations in simulations of aerosol effects, J. Geophys. Res. Atmos., doi:10.1002/jgrd.50432, 2013.

Wang, Y., Wang, M., Zhang, R., Ghan, S. J., Lin, Y., Hu, J., Pan, B., Levy, M., Jiang, J. H. and Molina, M. J.: Assessing the effects of anthropogenic aerosols on Pacific storm track using a multiscale global climate model, Proc. Natl. Acad. Sci. U. S. A., doi:10.1073/pnas.1403364111, 2014.

572 Wang, Y., Jiang, J. H., and Su, H.: Atmospheric responses to the redistribution of anthropogenic
573 aerosols, J. Geophys. Res.-Atmos., 120, 9625-9641, https://doi.org/10.1002/2015JD023665,
574 2015.
575 Wang, Y., P.-L. Ma, J. Jiang, H. Su and P. Rasch, Towards Reconciling the Influence of
576 Atmospheric Aerosols and Greenhouse Gases on Light Precipitation Changes in Eastern
577 China, J. Geophys. Res. Atmos. 121(10), 5878–5887, 2016.
578 Wang, Y., P. Ma, J. Peng, R. Zhang, J.H. Jiang, R. Easter and Y. Yung, Constraining Aging
579 Processes of Black Carbon in the Community Atmosphere Model Using Environmental
580 Chamber Measurements, J. Adv. Model. Earth Syst. 10(10), 2514-2526, 2018.
581 Wang, Y., Zheng, X., Dong, X., Xi, B., Wu, P., Logan, T., and Yung, Y. L.: Impacts of long-range
582 transport of aerosols on marine-boundary-layer clouds in the eastern North Atlantic, Atmos.
583 Chem. Phys., 20, 14741-14755, 10.5194/acp-20-14741-2020, 2020.
584 Wang, Y., Zheng, G., Jensen, M. P., Knopf, D. A., Laskin, A., Matthews, A. A., Mechem, D., Mei,
585 F., Moffet, R., Sedlacek, A. J., Shilling, J. E., Springston, S., Sullivan, A., Tomlinson, J.,
586 Veghte, D., Weber, R., Wood, R., Zawadowicz, M. A., and Wang, J.: Vertical profiles of
587 trace gas and aerosol properties over the eastern North Atlantic: variations with season and
588 synoptic condition, Atmos. Chem. Phys., 21, 11079-11098, 10.5194/acp-21-11079-2021,
589 2021.
590 Wu, P., Dong, X., Xi, B., Tian, J., and Ward, D. M.: Profiles of MBL Cloud and Drizzle
591 Microphysical Properties Retrieved From Ground-Based Observations and Validated by
592 Aircraft In Situ Measurements Over the Azores, J. Geophys. Res.-Atmos., 125, e2019JD032205,
593 https://doi.org/10.1029/2019JD032205, 2020.
594 Xie, S. C., Cederwall, R. T., and Zhang, M. H.: Developing long-term single-column model/cloud
595 system-resolving model forcing data using numerical weather prediction products constrained
596 by surface and top of the atmosphere observations, Journal of Geophysical Research-
597 Atmospheres, 109(D1), doi: 10.1029/2003jd004045, 2004
598 Yeager, S. G., Danabasoglu, G., Rosenbloom, N. A., Strand, W., Bates, S. C., Meehl, G. A.,
599 Karspeck, A. R., Lindsay, K., Long, M. C., Teng, H., and Lovenduski, N. S.: Predicting Near-
600 Term Changes in the Earth System: A Large Ensemble of Initialized Decadal Prediction
601 Simulations Using the Community Earth System Model, B. Am. Meteorol. Soc., 99, 1867-1886,
602 https://doi.org/10.1175/BAMS-D-17-0098.1, 2018.

603 Zawadowicz, M. A., Suski, K., Liu, J., Pekour, M., Fast, J., Mei, F., Sedlacek, A. J., Springston,
604 S., Wang, Y., Zaveri, R. A., Wood, R., Wang, J., and Shilling, J. E.: Aircraft measurements of
605 aerosol and trace gas chemistry in the eastern North Atlantic, Atmos. Chem. Phys., 21, 7983-
606 8002, 10.5194/acp-21-7983-2021, 2021.
607 Zhang, G. J. and McFarlane, N. A.: Sensitivity of climate simulations to the parameterization of
608 cumulus convection in the Canadian climate centre general circulation model, Atmosphere-
609 Ocean, 33, 407-446, 10.1080/07055900.1995.9649539, 1995.
610 Zhang, Z., Song, H., Ma, P.-L., Larson, V. E., Wang, M., Dong, X., and Wang, J.: Subgrid
611 variations of the cloud water and droplet number concentration over the tropical ocean: satellite
612 observations and implications for warm rain simulations in climate models, Atmos. Chem.
613 Phys., 19, 1077–1096, https://doi.org/10.5194/acp-19-1077-2019, 2019.
614 Zhao, L., Wang, Y., Zhao, C., Dong, X., and Yung, Y. L.: Compensating Errors in Cloud Radiative
615 and Physical Properties over the Southern Ocean in the CMIP6 Climate Models, Adv. Atmos.
616 Sci., 39, 2156-2171, 10.1007/s00376-022-2036-z, 2022.
617 Zhao, X., Liu, X., Phillips, V. T. J., and Patade, S.: Impacts of secondary ice production on Arctic
618 mixed-phase clouds based on ARM observations and CAM6 single-column model simulations,
619 Atmos. Chem. Phys., 21, 5685-5703, 10.5194/acp-21-5685-2021, 2021.
620 Zheng, X., Xi, B., Dong, X., Wu, P., Logan, T., and Wang, Y.: Environmental effects on aerosol–
621 cloud interaction in non-precipitating marine boundary layer (MBL) clouds over the eastern
622 North Atlantic, Atmos. Chem. Phys., 22, 335-354, 10.5194/acp-22-335-2022, 2022a.
623 Zheng, X., Dong, X., Ward, D. M., Xi, B., Wu, P., and Wang, Y.: Aerosol-Cloud-Precipitation
624 Interactions in a Closed-cell and Non-homogenous MBL Stratocumulus Cloud, Adv. Atmos.
625 Sci., 39, 2107-2123, 10.1007/s00376-022-2013-6, 2022b.
626

627 **Table 1**. Comparison of physical parameterizations relevant with warm cloud processes between
628 CAM5 and CAM6.
629

Model Physics	CAM5	CAM6
Cloud Microphysics	MG1 (*Morrison and Gettelman*, 2008) with KK scheme for warm rain processes.	MG2 with retuned autoconversion, explicit sub-grid variance of cloud, and prognostic rain and snow (*Morrison and Gettelman*, 2015)
Stratiform Macrophysics	The Park scheme (*Park et al.*, 2014)	The Cloud Layers Unified By Binormals (CLUBB), a prognostic moist turbulence scheme that unifies the representation of boundary layer, shallow convection, and stratiform macrophysics (*Golaz and Larson*, 2002)
PBL and shallow convection scheme	The University of Washington scheme (*Park and Bretherton*, 2009)	
Aerosol	3-mode Modal Aerosol Module (MAM3, *Ghan et al.*, 2011)	4-mode Modal Aerosol Module (MAM4) with a new "fresh-BC" mode (*Liu et al.*, 2016)

630

631 **Table 2**. Single-column numerical experiment design.

632

Model Physics	Experiment Name	Experiment Description
CAM6	Ctrl	Default model setup and forcing data
	D21	Using recalibrated warm rain parameterizations similar to Dong et al. (2021)
	pAero	Scale up aerosol number and mass concentrations in the accumulation mode by a factor of 2 in the initial condition
	ForcingQ_Adj	Adjust specific humidity state variable and related tendency terms by a factor of 0.85
CAM5	Ctrl	Default model setup and forcing data
	D21	Using recalibrated warm rain parameterizations based on Dong et al. (2021)

633

Figures

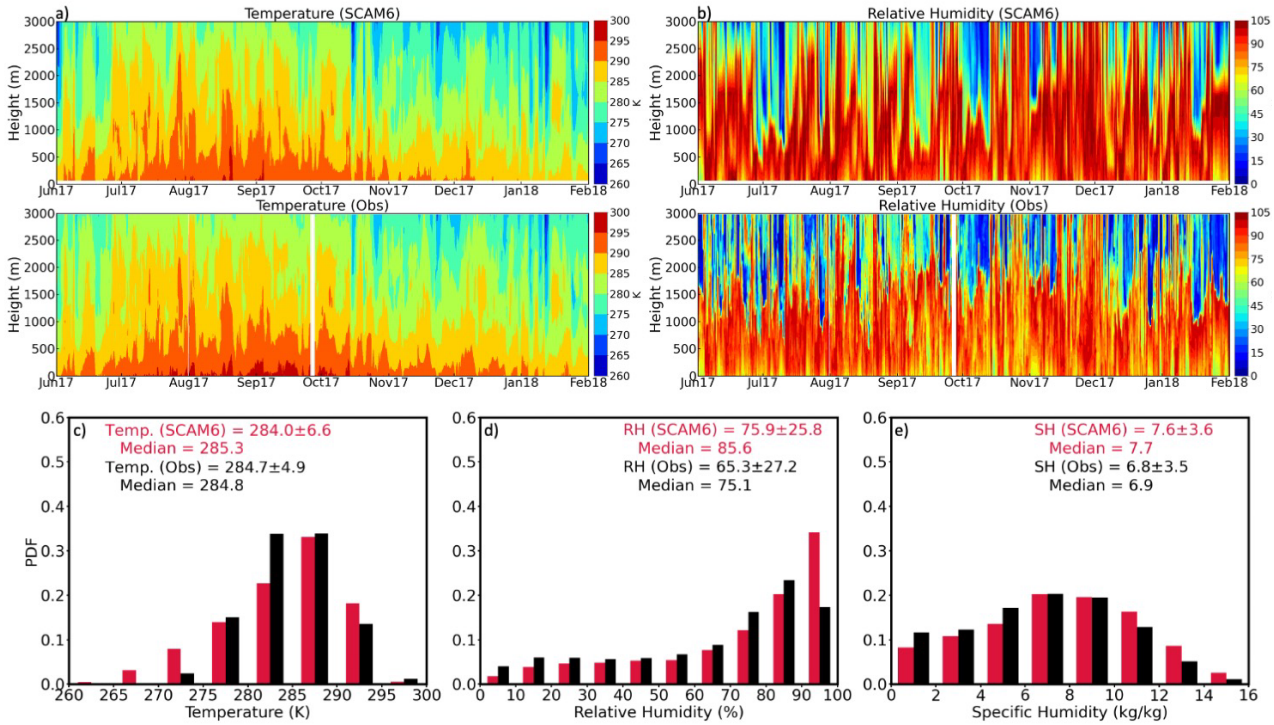

Figure 1. Comparisons of meteorological conditions between SCAM6 simulations and ARM Interpolated Sonde (INTERPSONDE) soundings. Upper panels: Time series of air temperature (left) and relative humidity (right) from SCAM6 (top) and ARM-ENA observations (bottom). Lower panels: SCAM6 (red) simulated air temperature, relative humidity (RH), specific humidity (SH) within 3 km, in comparison with the ARM-ENA observation (black).

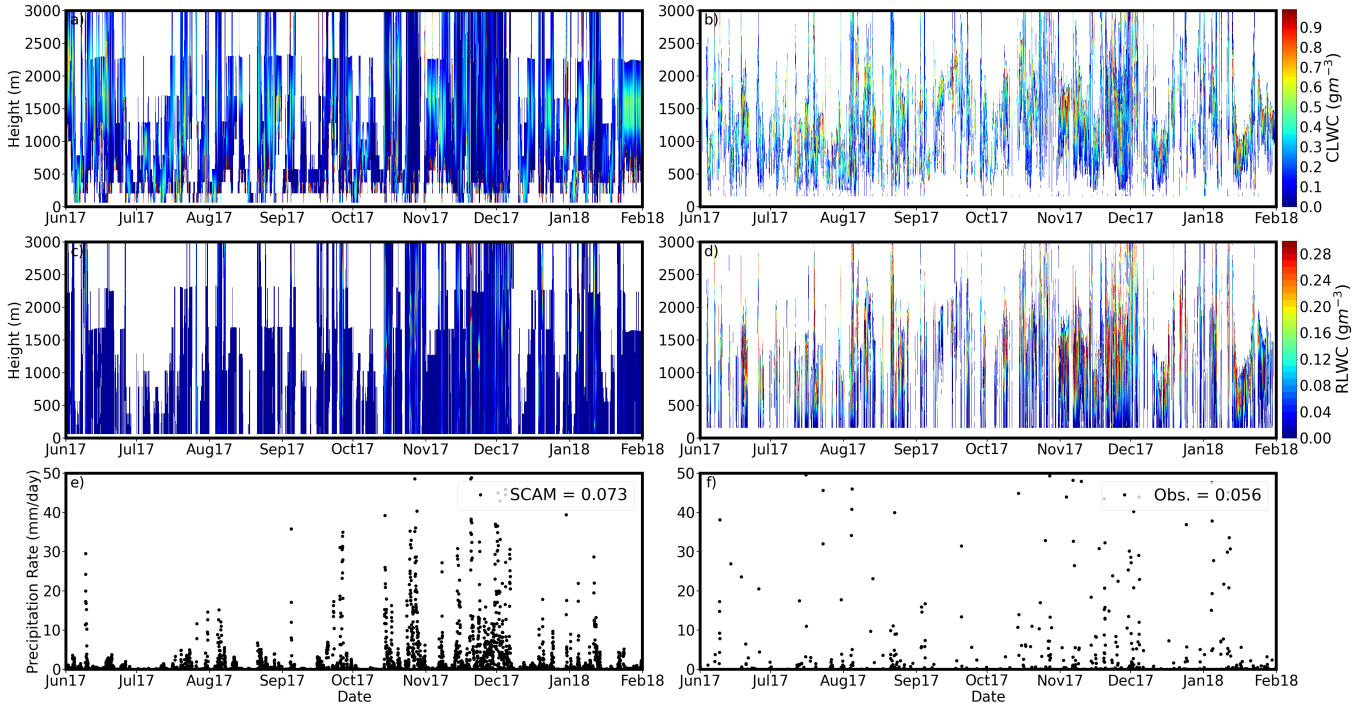

641

642 **Figure 2.** Time series of the cloud liquid water contents (CLWC, top panels), rain liquid water
643 contents (RLWC, middle panels) and surface precipitation (bottom panels) from the SCAM6
644 simulations (left column) and the ARM-ENA retrievals and observations (right column).

645

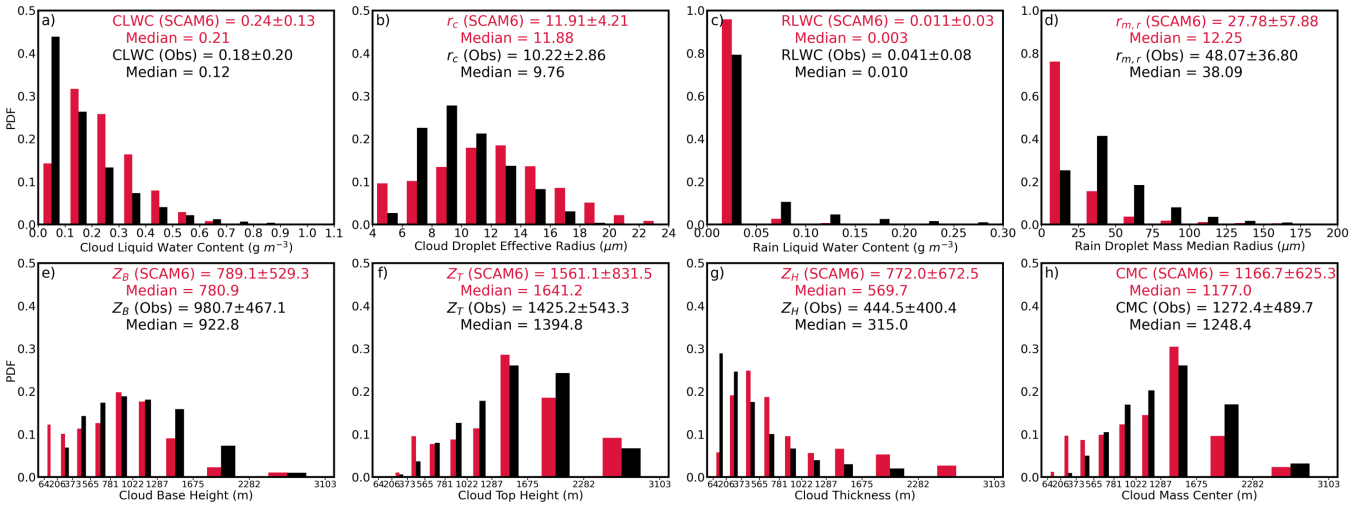

Figure 3. Probability distribution functions (PDFs), mean, standard deviation, and median values of cloud and rain microphysics, and cloud macrophysics simulated from SCAM6 (red) and observed/retrieved from ground-based remote sensors (black). (a) Cloud liquid water content, CLWC; (b) Cloud droplet effective radius, r_c; (c) Rain liquid water content, RLWC; (d) Rain droplet mass median radius, $r_{m,r}$; (e) Cloud base height, Z_B; (f) Cloud top height, Z_T; (g) Cloud thickness, Z_H and (h) Cloud mass center.

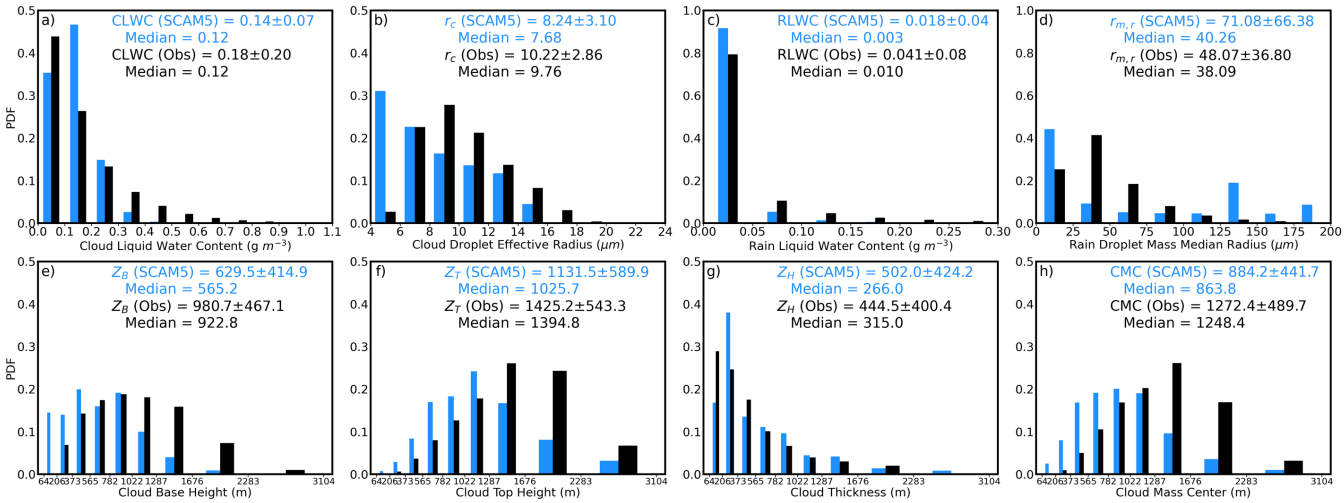

654

655 **Figure 4**. Same as Fig 3, except for SCAM5 (blue).

656

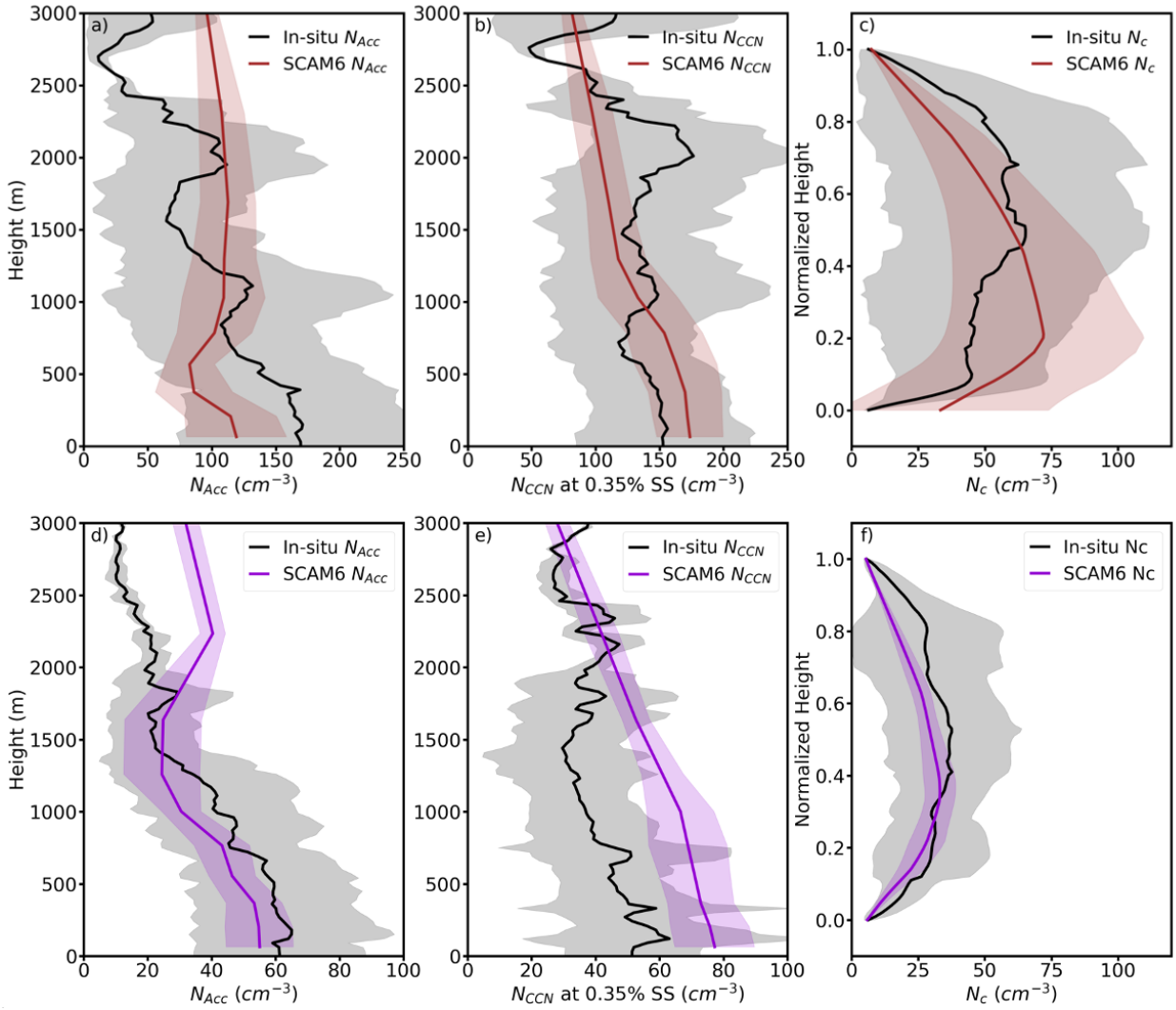

Figure 5. Vertical profiles of accumulation mode aerosol (N_{ACC}) (a, d); CCN concentration (N_{CCN}) at 0.35% supersaturation (b, e) during interstitial conditions, and Cloud droplet number concentration (N_c) at normalized height (c, f, 0 is cloud base, 1 is cloud top) for cloudy samples. For SCAM6 simulations (brown and purple) and aircraft in situ measurement (black), during the Summer (top panels) and Winter (bottom panels) ACE-ENA IOPs. The shaded areas denote the standard deviation at each level. The SCAM6 simulations are selected within each time duration of the aircraft cases. The reason of using normalized height for N_c is that the cloud layer thickness and vertical positions differ for each corresponding time stamp. We need to normalize the height within each cloud layer to ensure that the N_c vertical variation is representative.

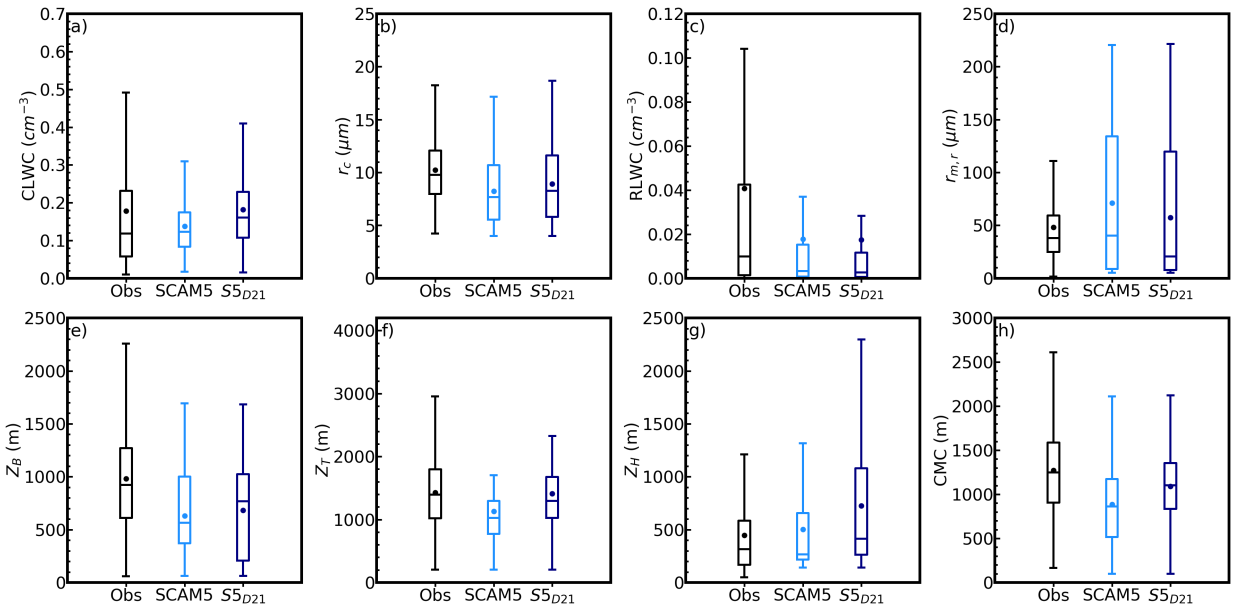

668

669 **Figure 6**. Comparisons of cloud and rain microphysics, and cloud macrophysics between
670 observations (black), SCAM5 (blue) and SCAM5 with Dong2021 parameterization ($SCAM5_{D21}$,
671 dark blue). (a) $CLWC$, (b) r_c, (c)$RLWC$, (d) $r_{m,d}$, (e) Z_B, (f) Z_T, (g) $Z_{H,}$ and (h) Cloud mass center.
672 Dots represent the mean values, and the bars from bottom to top represent 10%, 25%, 50%, 75%,
673 and 90% values, respectively.

674

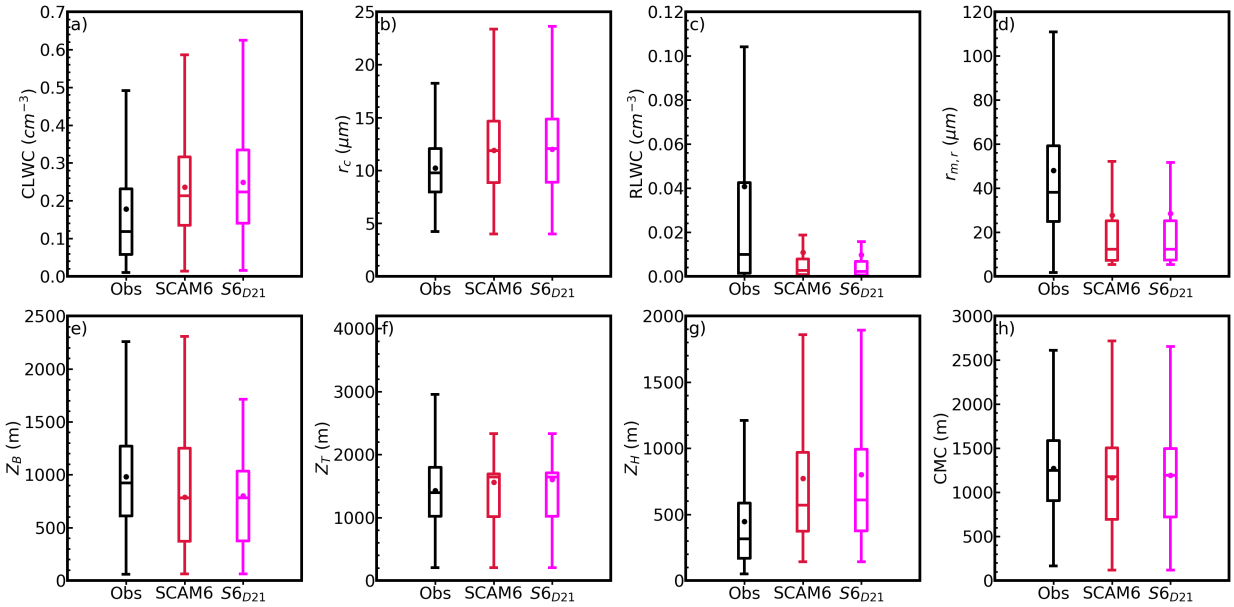

675

676 **Figure 7**. Same as Fig 6, except for SCAM6 (red), and SCAM6 with Dong2021 parameterization

677 ($SCAM6_{D21}$, pink).

678

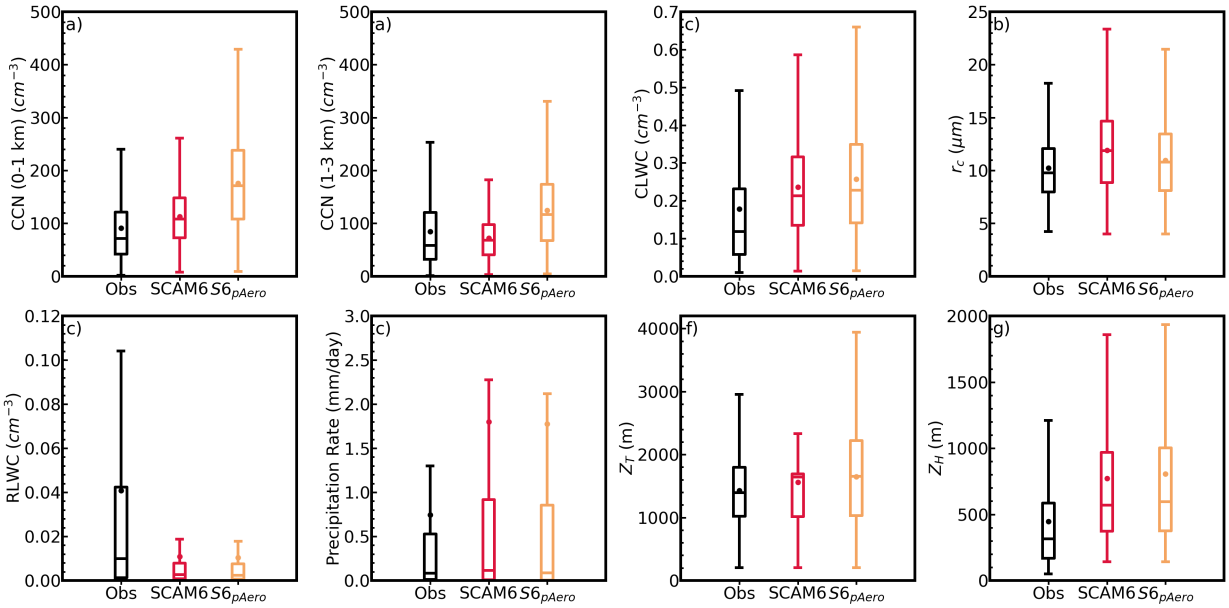

Figure 8. Aerosol and cloud properties simulated from control (red) and aerosol-perturbing experiments (pAero, orange) by SCAM6 and comparison to observations. The observed CCN at 0.35% SS are averaged from the selected aircraft measurements during the ACE-ENA.